Article

Functional Rearrangement of the Light-Harvesting Antenna upon State Transitions in a Green Alga

Lucyna M. Wlodarczyk,[1,*] Joris J. Snellenburg,[1] Janne A. Ihalainen,[2] Rienk van Grondelle,[1] Ivo H. M. van Stokkum,[1] and Jan P. Dekker[1]

[1]Department of Physics and Astronomy, Faculty of Sciences, VU University Amsterdam, Amsterdam, The Netherlands; and [2]Nanoscience Center, Department of Biological and Environmental Science, University of Jyväskylä, Jyväskylä, Finland

ABSTRACT State transitions in the green alga *Chlamydomonas reinhardtii* serve to balance excitation energy transfer to photosystem I (PSI) and to photosystem II (PSII) and possibly play a role as a photoprotective mechanism. Thus, light-harvesting complex II (LHCII) can switch between the photosystems consequently transferring more excitation energy to PSII (state 1) or to PSI (state 2) or can end up in LHCII-only domains. In this study, low-temperature (77 K) steady-state and time-resolved fluorescence measured on intact cells of *Chlamydomonas reinhardtii* shows that independently of the state excitation energy transfer from LHCII to PSI or to PSII occurs on two main timescales of <15 ps and ~100 ps. Moreover, in state 1 almost all LHCIIs are functionally connected to PSII, whereas the transition from state 1 to a state 2 chemically locked by 0.1 M sodium fluoride leads to an almost complete functional release of LHCIIs from PSII. About 2/3 of the released LHCIIs transfer energy to PSI and ~1/3 of the released LHCIIs form a component designated X-685 peaking at 685 nm that decays with time constants of 0.28 and 5.8 ns and does not transfer energy to PSI or to PSII. A less complete state 2 was obtained in cells incubated under anaerobic conditions without chemical locking. In this state about half of all LHCIIs remained functionally connected to PSII, whereas the remaining half became functionally connected to PSI or formed X-685 in similar amounts as with chemical locking. We demonstrate that X-685 originates from LHCII domains not connected to a photosystem and that its presence introduces a change in the interpretation of 77 K steady-state fluorescence emission measured upon state transitions in *Chalamydomonas reinhardtii*.

INTRODUCTION

Photosystem I (PSI) and photosystem II (PSII) are pigment-protein complexes that perform primary photochemistry in oxygenic photosynthesis. A large part of the photons required to drive photosynthesis is absorbed by so-called light harvesting complex bound to PSI (LHCI) or to PSII (LHCII) (1), and resulting excitations are subsequently efficiently transferred to the reaction center of the respective photosystems (PSs), where charge separation occurs (2–5). Steady electron flow in the downstream electron transport chain coupled to PSII and PSI is essential for efficient photosynthesis and requires a process that deftly provides a careful balance in the amount of excitations arriving at PSI and PSII, which have slightly different spectral responses. The process that allows photosynthetic organisms to adjust the unbalanced excitation is called state transitions (ST) (6–8). The general idea is as follows: 1) predominant excitation of PSII over PSI leads to an increased reduction of the plastoquinone (PQ) pool in the electron transport chain by electrons originating from PSII; 2) this results in the activation of a kinase via cytochrome b_6f (9); 3) the active kinase phosphorylates LHCII, causing its disassociation from PSII; and 4) subsequent attachment to PSI. As a result, more excitation energy reaches PSI at the expense of PSII, thereby restoring the excitation balance between the PSs (10,11). The arrangement of the photosynthetic apparatus where LHCII is phosphorylated and functionally attached to PSI is called state 2 (S2). The process is reversible—LHCII is dephosphorylated by an invariably active phosphatase, thus PSII can become again the main receiver of the excitation energy absorbed by LHCII, a condition called state 1 (S1) (12,13). The fitness of photosynthetic organisms, which evolved the capability of undergoing ST is highly dependent on this regulatory process, therefore studies aiming at better understanding ST are essential.

In this work, we studied ST in a green unicellular alga *Chlamydomonas reinhardtii* (*C.r.*), a model organism used extensively in photosynthesis research (14). Interestingly, although ST in plants involve 15–20% of LHCII (8,15), in *C.r.* the respective amount has been measured to reach even 80% (16). A different degree of stacking of photosynthetic membranes in plants versus *C.r.* (17,18) and the presence of CP29 in the LHCII-PSI complex of *C.r.* (19,20). but not of plants (21) pose possible reasons for the difference in magnitude of ST between plants and *C.r.* Additionally, it has

Submitted September 3, 2014, and accepted for publication November 26, 2014.

*Correspondence: l.m.wlodarczyk@vu.nl

Lucyna M. Wlodarczyk and Joris J. Snellenburg contributed equally to this work.

Editor: Leonid Brown.

0006-3495/15/01/0261/11 $2.00

http://dx.doi.org/10.1016/j.bpj.2014.11.3470

been suggested in a number of studies that ST in *C.r.* might also play a role in a switch between linear and cyclic electron flow (22,23), however this connection was recently questioned (24).

Recently, two studies were published in which ST in *C.r.* were studied by noninvasive spectroscopic methods on intact cells (25,26). Both studies showed that upon the S1 → S2 transition, the decrease of the antenna size of PSII is much larger than the increase of the antenna size of PSI, suggesting that not all LHCII is involved in migration from PSII to PSI. Instead it was postulated that a part of the antenna that detaches from PSII organizes itself into domains of uncoupled LHCII, which presence was suggested also before (27). These unbound LHCII complexes exhibit shorter excited state lifetimes and thereby protect themselves against photodamage (28).

In this work we extend the analysis of ST in *C.r.* by noninvasive methods by 1) steady-state fluorescence emission (77 K and 6 K) and excitation (77 K) spectroscopy and 2) time-resolved fluorescence spectroscopy at 77 K, probing fluorescence spectral evolution on an ultrafast timescale (few ps to few ns) (29). Changes in the photosynthetic apparatus upon ST affect excitation energy transfer (EET) pathways, resulting in differences in the kinetics of the fluorescence emission of the system (30), thus, time-resolved fluorescence is a useful technique to study ST. The measurements were analyzed globally and a target model was constructed. The structural implications for the reorganization of the thylakoid membrane are discussed.

MATERIALS AND METHODS

Strain and growth conditions

Chlamydomonas reinhardtii wild-type (WT) and *stt7* mutant were a kind gift of Prof. Jean-David Rochaix. The WT and *stt7* cells were grown under 25 μmol photons PAR m^{-2} s^{-1} illumination in Tris-acetate-phosphate medium at 25°C with constant mixing (170 rpm) on an incubator shaker (Minitron, INFORS HT). Measurements were performed on the cells in a mid-logarithmic phase of growth (OD_{750} ~0.7). Under these conditions the cells were naturally in S1 as it has been shown before (31).

Induction of state transitions

State 1 was induced in the cells strongly aerated in the dark for 90 min in the presence of 0.1 μM staurosporine, a kinase inhibitor that prevents phosphorylation of LHCII (32). This chemically locked state 1 is further denoted as **S1c**. Alternatively, no kinase inhibitor was used and cells were strongly aerated for 30 min under >720 nm light to preferentially excite PSI and hence oxidize the PQ pool, thus with no chemical locking this state 1 is further denoted as **S1nc**. For state 2, cells were incubated 45 min under anaerobic conditions in the dark, conditions which lead to reduction of the PQ pool (33–36). This way of S2 induction is well justified taking into account that *C.r.* experiences anaerobic conditions also naturally (37) and is further denoted as **S2nc** (no chemical locking). A stronger state 2 was obtained when sodium fluoride (0.1 M) was also present during incubation to inhibit dephosphorylation of LHCII (32) and this chemically locked state 2 is further denoted as **S2c**. *Stt7* mutant demonstrates impaired phosphorylation of LHCII, thus it is locked in state 1 (11).

Spectroscopic measurements

Steady-state fluorescence emission and excitation spectra and time-resolved fluorescence measurements were performed at 77 K. For the measurements cell suspensions were diluted to a final chlorophyll concentration of below 1 μg/ml. After induction of S1 or S2, intact *C.r.* cells were instantly frozen in the presence of glycerol as cryoprotectant (65% v/v) in nitrogen cryostat (Oxford Instruments, Abingdon, United Kingdom). The optical density (A680–A750) was invariably below 0.1 and the respective values were used to normalize the steady-state fluorescence spectra. Fluorescence emission and excitation spectra were measured with a Fluoro-Log Tau-3 (Jobin Yvon, HORIBA, Kyoto, Japan). Samples were excited at 475 nm and spectral resolution was 0.5 nm both for emission and excitation spectra. The latter spectra were measured at 695 nm (primarily PSII emission) or at 715 nm (primarily PSI emission).

Time-resolved fluorescence measurements were performed with a synchroscan streak camera setup. Excitation pulses of ≈100 fs width and centered at 475 nm (5.0 ± 1.0 nm full-width at half maximum) were generated with a titanium:sapphire oscillator (VITESSE, Coherent, Santa Clara, California), which served as a seed for an ultrafast regenerative amplifier (REGA, Coherent, Santa Clara, California) followed by a double pass optical parametric amplifier (OPA, Coherent, Santa Clara, California). The repetition rate was 50 kHz and the energy per pulse was 14 nJ (for S1c and S2c) or 6 nJ (for S1nc and S2nc). The resulting laser beam was focused on the sample giving a spot of ≈150 μm in diameter. Fluorescence was detected at a right angle to the excitation beam using a Chromex 250IS spectrograph (Chromex, Albuquerque, New Mexico) and a Hamamatsu C5680 synchroscan camera (Hamamatsu Photonics, Hamamatsu, Japan). Scattered laser light was cut off by an orange glass filter OC11. Finally, the streak images were recorded on a cooled Hamamatsu Digital Camera C10600-10B (ORCA-R^2) (Hamamatsu Photonics, Hamamatsu, Japan). To account for lifetimes ranging from a few ps up to a few ns, each sample was measured in three time-windows of ≈150 ps, ≈400 ps, and ≈1.5 ns. The full-width at half maximum of the time response in the shortest time range was ≈4 ps. The spectral range of each image was 270 nm (550–820 nm) with a wavelength resolution of ≈4 nm. Preceding the global and target analyses, the measured streak images were background subtracted and corrected for a wavelength dependent sensitivity of the detector (shading correction), all that was done using Hamamatsu High Performance Digital Temporal Analyzer (HPD-TA) 8.2.0.

Global analysis (GA) and target analysis (TA)

In GA the time-resolved data is fitted as the sum of a number n_{comp} of exponential decays with rate constant k_l (reciprocal of the lifetime), convolved with the instrument response function and multiplied by the corresponding amplitude of the decay at each recorded wavelength (λ) as represented by the so-called decay associated spectra (DAS). The fitted data $\Psi(t,\lambda)$ can then be written as

$$\Psi(t,\lambda) = \sum_{l=1}^{n_{comp}} (\exp(-k_l t) \otimes \mathrm{IRF}(t)) DAS_l(\lambda).$$

In addition to a number of independent decays constituting a parallel scheme, more complex schemes are possible. The next simplest scheme is the unbranched, unidirectional model ($1 \rightarrow 2 \rightarrow \ldots \rightarrow n_{comp}$) where the individual components, also called compartments, decay sequentially. In this so-called sequential scheme, the first compartment gets populated by an input (the excitation pulse) and as it decays, it forms the second component. The second component then decays into the third component, etc. The corresponding estimated spectral amplitudes are called the evolution associated spectra. For a certain n_{comp} number of components the parallel scheme and the sequential schema are mathematically equivalent, resulting in the exact same fit. An even more complex scheme, combining both sequential and parallel elements as well as imposing spectral relations such as zero constraints, spectral equality and/or equal area constraints is the basis for TA

(38,39). A compartmental scheme is constructed to test some specific photophysical or photochemical model. In this case the corresponding estimated spectral amplitudes are called the species associated spectra (SAS), reflecting the specific functional role in the photophysical or photochemical model each species corresponds to. In TA multiple measurements of the same system in different experimental conditions (different temperatures, pH, or excitation energy), different biological conditions (such as green algae cells poised in state 1 or state 2), or different systems (mutants) under identical experimental conditions can be combined. In this way more information about the system can be extracted from the data than by GA of the individual experiments. In this work the target model specifically allowed to quantify the amount of LHCII involved in ST and the percentage of EET to either PSI or to PSII or being quenched in S1 or in S2 at 77 K.

RESULTS

All present measurements were performed at cryogenic temperatures on intact, instantly frozen *C.r.* cells poised in S1 or in S2 to ensure that the photosynthetic apparatus was intact and a reversal of ST did not occur (e.g., due to measuring conditions). In addition, at the low temperatures most PSs and LHCs have more distinguishable spectroscopic properties, which allow a better identification of the energy transfer and charge separation processes in the intact cells.

77 K steady-state fluorescence emission and excitation spectra

To qualitatively assess ST, we first recorded steady-state fluorescence spectra at 77 K of intact *C.r.* cells where state 1 and state 2 were locked chemically (S1c and S2c, respectively) or where no inhibitors were used to lock the respective states (S1nc and S2nc). The spectra are depicted in Fig. 1 (except for the S1nc spectrum, which was very similar to the S1c spectrum).

Independent of the state, upon excitation at 475 nm (where mainly Chl *b* and carotenoids were excited) three emission maxima appear that presumably originate from PSI (≈712 nm) and PSII (≈685 and ≈695 nm). In S1c the fluorescence spectrum is dominated by emission originating from PSII, whereas the transition to S2c causes a pronounced increase of the PSI emission. This can be qualitatively observed by an increase in the emission at 712 nm, accompanied by a much smaller decrease around 685 and 695 nm. This change is particularly significant when phosphatase inhibitor was used to lock the cells in state 2 (S2c). The less pronounced increase of emission ≈712 nm observed in S2nc in comparison to S2c suggests that two different types of state 2 were induced in the two samples.

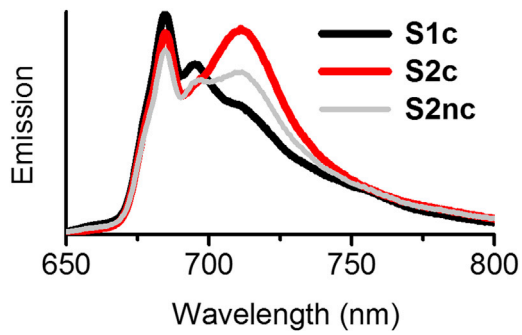

FIGURE 1 The 77 K steady-state fluorescence emission spectra of intact instantly frozen WT *C.r.* cells chemically locked in state 1 (S1c, *black*) or in state 2 (S2c, *red*) or upon state 2 induction without subsequent chemical locking (S2nc, *gray*). The excitation was at 475 nm and the spectra were OD normalized. Note that upon S1c → S2c transition the emission commonly attributed to PSII (maxima at ≈685 and ≈695 nm) decreases slightly and is accompanied by a significant increase in emission originating from PSI (≈715 nm). To see this figure in color, go online.

We also recorded 77 K steady-state excitation spectra at 715 nm and at 695 nm on cells chemically locked in state 1 (S1c) or in state 2 (S2c). The results of these measurements are shown in the Supporting Material (Fig. S1). To further elucidate on the difference between state 1 and state 2, we also measured fluorescence emission spectra of thylakoid membranes of *C.r.* at 6 K and discuss them in the Supporting Material (Fig. S2).

Global analysis of the time-resolved fluorescence emission at 77 K

Upon excitation at 475 nm (selectively exciting Chl *b* and carotenoids) using a streak camera setup, we measured the spectral evolution of the emission from intact *C.r.* cells in state 1 or in state 2 treated with kinase or phosphatase inhibitor (S1c and S2c, respectively) and not locked chemically (S1nc and S2nc) (29). S1nc and S1c yield virtually identical results, therefore only S1c is further discussed as a state 1 representative. The evolution of fluorescence spectra obtained for S1c, S2nc, and S2c is shown in Fig. S3. The resulting data was analyzed by means of GA using the freely available software package Glotaran (40). It was found that the fluorescence decay in S1c, S2c, and S2nc is satisfactorily fitted using a total of five components. The DAS depicted in Fig. 2 *A* (S1c) and in Fig. 2 *B* (S2c) represent the amplitudes of each component over the whole recorded spectral range. Likewise, the DAS obtained when no inhibitors were used to lock a respective state are shown in Fig. S5. Noteworthy, our results are in line with previously reported 77 K fluorescence time-resolved data for spinach and cyanobacteria (39,41,42).

Kinetic traces at four representative wavelengths of data measured for S1c and S2c along with fits are depicted in Fig. S4. In these traces the S1 → S2 transition is apparent as a relative decrease of fluorescence at PSII characteristic wavelengths (685 and 695 nm) concomitant with an increase in fluorescence at PSI characteristic wavelengths (712 and 720 nm). This information, combined with the knowledge that the respective difference in loss and rise is likely to be attributed to the loss and gain in LHCII antenna

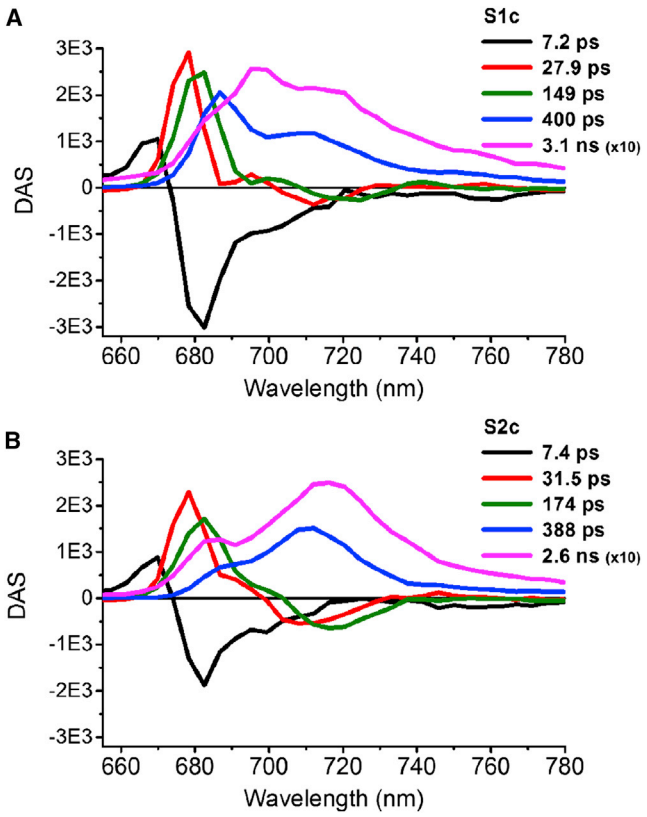

FIGURE 2 DAS estimated from GA of 77 K time-resolved fluorescence emission spectra of intact instantly frozen WT *C.r.* cells chemically locked in state 1 (S1c) or in state 2 (S2c). The decay and rise in the 30-ps (*red*) and 160-ps (*green*) DAS reflects EET from LHCII to PSs. The DAS of the longest two lifetimes (*blue and magenta*), representing a mixture of PSI and PSII emission show clear changes upon state transition. To see this figure in color, go online.

functionally connected to a corresponding PS, will be further used in the target model.

Independently of the state, a component with the shortest decay time of 7 ps is characterized by a fluorescence loss at 670 nm accompanied by a much larger fluorescence increase at 682.5 nm (Fig. 2, *black*). We interpret this DAS as energy transfer from blue Chl *a*, Chl *b*, or carotenoid states to Chl *a* states that are lower in energy. The apparent nonconservativity is most likely caused by energy transfer on a similar transfer timescale from states emitting outside of the measured spectral range to Chl *a*.

The effect of ST on the EET in the studied system occurs in the second component (Fig. 2, *red*). In both states the DAS characterizing a ≈30-ps decay has a maximum at 678 nm, suggesting decay of LHC components. The negative feature at around 710 nm, caused by an increase of fluorescence arising from red chlorophylls in PSI, is more prominent in S2c than in S1c. Concomitantly, the dip at ~690 nm, presumably caused by an increase of fluorescence arising from the 690 nm chlorophyll in the CP47 core antenna of PSII, is much clearer in S1c than in S2c. Taking into account that emission around 690 nm originates mainly from PSII and that PSI dominates the emission at 710 nm, these data indicate that on a timescale of 30 ps PSII receives more excitation energy in S1c in comparison to S2c, whereas in S2c PSI receives more excitation energy.

The next DAS represents decays of 149 ps in S1c and 174 ps in S2c (Fig. 2, *green*). After peaking at ≈682 nm (both states), the DAS decreases and forms a broad negative band with a minimum at ~716 nm. Apart from a red shift, these spectra closely resemble the DAS of the 30-ps component. Hence, a negative feature around 695 nm in the red flank of the positive band at 682 nm appears to be more pronounced in S1c. Moreover, upon transition to S2c the negative band at ~716 nm increases. Therefore, we suggest that this component is also caused by EET from LHCII ultimately toward red-shifted chlorophylls in either PSII (695 nm) or PSI (716 nm).

The fourth DAS has positive contributions at around 687 and 712 nm, both in S1c (400 ps) and in S2c (388 ps), indicating loss of fluorescence, either due to charge separation in PSII or in PSI, or to decay of the excited state in an antenna complex that cannot transfer energy to one of the PSs (Fig. 2, *blue*). If the latter were true, this antenna complex must be in a quenched configuration (in view of the ≈400 ps lifetime). This process of excitation energy trapping is preceded by slow uphill energy transfer from the PSII antenna to the PSII core complex (maximum at 687 nm) or from the PSI antenna to the PSI core complex (maximum at 712 nm). The amplitudes of the peaks in the DAS change depending on the amount of energy transferred toward both PSs in the ≈30 and ≈160 ps phases, hence the shape of the DAS describing the ≈400 ps decay reflects the extent of ST.

Decay of fluorescence throughout the spectrum is observed also in the fifth DAS (Fig. 2, *magenta*). In S1c the component has a decay time of 3.1 ns and is characterized by a maximum at 695 nm accompanied by shoulders both on the blue side (687 nm) and on the red side (712 nm). This spectrum describes mainly the decay of excitations trapped by the red-absorbing chlorophylls in CP47 (maximum at 695 nm) (43) and trapping by the red-absorbing chlorophylls in LHCI or the PSI core (band around 712 nm) (41). Upon transition to S2c the DAS around 690 nm is clearly reduced at the expense of the pronounced maximum around 712 nm. This red-shift indicates an increased contribution of red chlorophylls of PSI. The lifetime of this component in S2c is 2.6 ns, which is very close to a time constant of 2.3 ns reported before for a trapping component of PSI-200 complexes from spinach (41). Note that a shoulder is present at 685 nm.

Summarizing, in our GA of the time-resolved fluorescence data there are two components with lifetimes of ≈30 ps and ≈160 ps reflecting changes in the EET from LHCII to the PSs (Fig. 2). Similar results are observed when state 1 and state 2 were not locked chemically

(Fig. S5), however the respective lifetimes obtained in S2nc are slightly shorter (22 ps and 140 ps). The difference in EET from LHCII to the PSs poses a base for subsequent target analysis where it provides the additional resolving power to separate PS I and PS II emission and to make quantitative statements on the nature of the state transition, which is not possible using GA alone.

Target analysis of the time-resolved fluorescence emission at 77 K

TA describes the kinetics of the compartments (ensembles of pigments sharing the same spectroscopic features and functional role) as well as the connectivity (meaning the transfer of excitation energy) between these compartments. A model used to simultaneously describe the 77 K time-resolved fluorescence emission in state 1 and in state 2 consists of two main parts (Fig. 3).

The first part of the model describes the functional connectivity of LHCII attached to either PSII or PSI. In parallel LHCII, which is not connected to either PSI or to PSII, is introduced (X-685). The second part of the model describes the spectral evolution of PSI and PSII without attempting to resolve the underlying equilibria, an approach previously used to describe the dynamics of energy transfer in stacked versus unstacked thylakoid membranes from spinach (39). In that study, upon unstacking of the thylakoid membranes a large increase in PSI characteristic emission, concomitant with a decrease in PSII characteristic emission was also observed. The input to the different components in state 1 and in state 2 (the amount of light absorbed by LHCII, PSI, PSII, and X-685) as well as the extent of the "fast" and "slow" energy transfer processes from LHCII to the PSs are collated in Table 1 (for S1c, S2c, and S2nc).

Note that the target model, which is shown in Fig. 3, is similar independently of whether or not the respective states were locked chemically. The corresponding population profiles and SAS are shown in Fig. 4 (S1c and S2c) and in Fig. S6 (S1nc and S2nc). The assumption of fast and slow energy transfer processes from LHCII to the PSs is justified by the results of the GA, whereas the addition of the X-685 compartment is justified by the results from the 6 K emission spectra (Fig. S2 and Table S1). Thus, the current model consists of four components (LHCII, PSII, PSI, and X-685) with nine spectra: LHCII, X-685 and—to describe the spectral evolution of PSs—three for PSII (the PSII core complex plus the firmly associated minor antenna complexes) and four for PSI (the PSI core complex plus the LHCI antenna). In the following we describe the characteristics of the four main components.

LHCII

For *C.r.* cells in S1c, we estimated that 68% of the excitation energy at 475 nm is absorbed by LHCII (Table 1 and Fig. 3). At this wavelength the Chl *b* absorption is much larger than

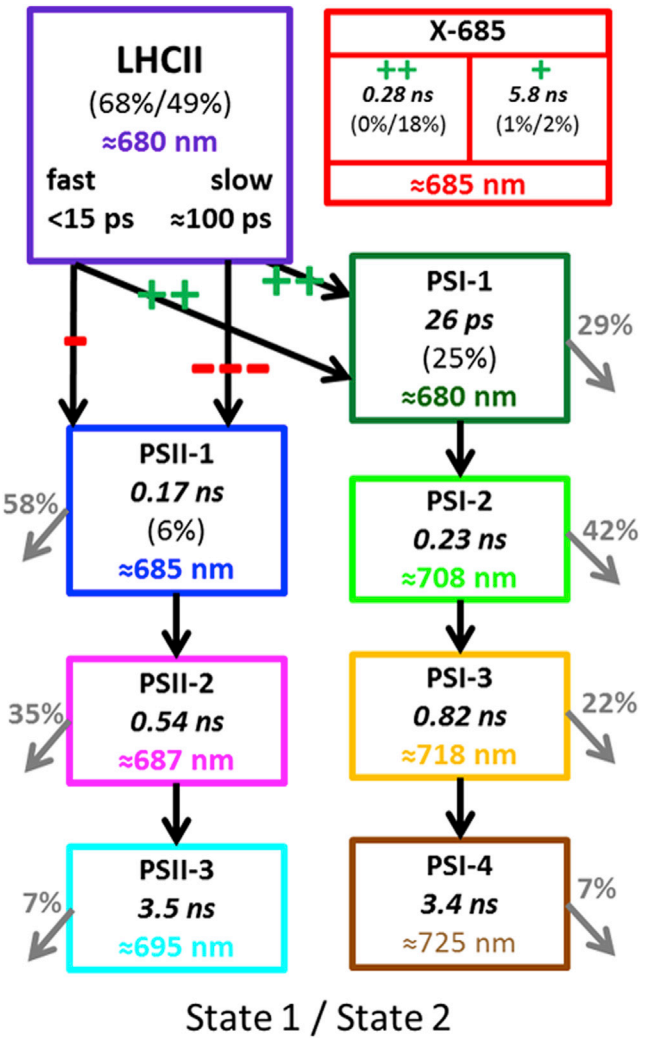

FIGURE 3 Kinetic scheme for LHCII, X-685 and the PSs of *C.r.* cells at 77 K described in the main text. The pluses and minuses indicate the change in energy transfer from LHCII to the PSs upon S1c → S2c transition (for PSI and PSII) or the change in population from the precursor (for X-685). The exact numbers are collated in Table 1. Gray arrows correspond to trapping on the PSs. To see this figure in color, go online.

that of Chl *a*. Although carotenoids also absorb here, the amount of Chl *b* in the various complexes will dominate the absorption at this wavelength. The PSI-LHCI complex contains ~44 Chl *b* (44), whereas the minor antenna complexes CP29 and CP26 associated with PSII contain just a few Chl *b* molecules. Furthermore, there are ~7 LHCII trimers per PSII monomer, and the ratio of PSII/PSI is ~1:1 (31,44). With 6.15 Chl *b* per LHCII monomer this means that ~138 Chl *b* molecules (or 73%) are associated with LHCII. Taking into account some absorption by carotenoids and Chl *a* at 475 nm, the number of 68% seems reasonable.

Fig. 4 *B* shows the SAS of the LHCII compartment (*purple*). It has a large peak at 681 nm with a characteristic vibrational tail. A ≈20% loss in the input into this compartment in S2c vs. S1c (Table 1) is visible as a lower maximum

TABLE 1 Input to the different compartments in states S1c, S2c, and S2nc, and distribution of LHCII input to the PSs

Inputs	S1c (%)	S2c (%)	S2nc (%)
PSI core + LHCI	25	25	25
PSII core + CP29/CP26	6	6	6
X-685	1	20 ± 3	17 ± 5
LHCII	68 ± 3	49 ± 3	52 ± 5
LHCII-fast → PSII	15	4	9
LHCII-fast → PSI	3	16	10
LHCII-slow → PSII	50	0	24
LHCII-slow → PSI	0	29	9

The standard error of the fitted input parameters is <2% unless otherwise indicated. The bottom four rows are estimated with a relative precision of 10%. The errors in the LHCII percentages for the S1c and S2c column are 3% and for S2nc the errors are 5% due to a lower signal/noise ratio of those data.

reached of the population profile (*dashed versus solid purple line* in Fig. 4 *A*). Similar SAS of the LHCII are obtained for states not locked chemically (Fig. S6), however upon S1nc → S2nc transition its population decreases less, by ≈16% (Table 1).

In S1c, almost all LHCII complexes transfer excitation energy to PSII on the "slow" timescale of ~100 ps (50 out of 68%, see Table 1), but a minor part (15 out of 68%) transfer on a "fast" timescale. It is possible that LHCII complexes directly associated with PSII (at the S, M, and N binding sites (44)) dominate the faster energy transfer times, and that those complexes that are located at longer distances (including those at the opposing side in a grana stack) dominate the slower energy transfer times. The model furthermore suggests that only a very small part of the LHCII complexes transfer energy to PSI on the fast timescale (3 out of 68%), and none on the slower timescale (Table 1).

In S2c the situation is radically different: less LHCIIs transfer excitation energy to the PSs (49% vs. 68% in S1, see Table 1) and the remaining LHCII is now found in the red-shifted X-685 compartment (20%). The LHCII that still transfers energy to the PSs, transfers it primarily to PSI (16 out of 49% as "fast" and 29 out of 49% as "slow"). Only a small part of the LHCII complexes transfer excitation energy to PSII (4 out of 49%). Less pronounced changes are observed for S2nc: 52% of excitation energy is transferred to PSs via LHCII from which 19% reaches PSI and 33% reaches PSII, thus upon S1nc → S2nc transition PSII remains the main receiver of excitation energy arriving from LHCII. Additionally, also here there is a pool of LHCII that gives rise to X-685 (17%).

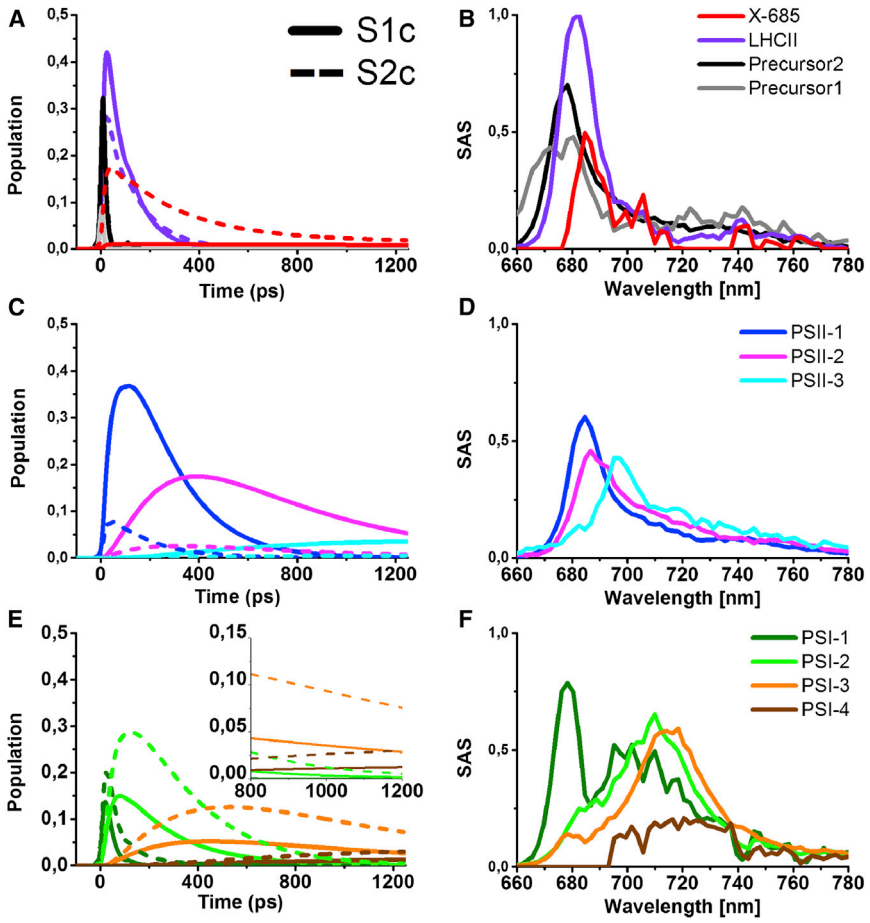

FIGURE 4 Population profiles (*A*, *C*, and *E*) and corresponding SAS (*B*, *D*, and *F*) estimated from the target model (Fig. 3) of the 77 K time-resolved fluorescence emission spectra of intact instantly frozen WT *C.r.* cells chemically locked in state 1 (S1c) or in state 2 (S2c). To see this figure in color, go online.

PSII

Only a small fraction of the light is absorbed by the PSII core complex and the associated antenna complexes CP26 and CP29 (6%). Fig. 4, *C* and *D*, show respectively the dynamics and spectral evolution of the PSII compartments. The compartments are characterized by the three characteristic bands and their vibrational tail typically observed at 77 K. PSII-1 represents predominantly the emission coming from a significant part of the PSII core chlorophylls (peaking at ~685 nm) that disappears (presumably because of trapping by charge separation) on a timescale of ~170 ps (Fig. 3). The timescale of this emission resembles that of a major trapping component in thylakoid membranes from spinach at 77 K (39), though the emission maximum is considerably red-shifted in *C.r.* (684 nm) compared to spinach (679 nm). The PSII-2 compartment has a lifetime of ~0.5 ns both in *C.r.* (Fig. 3) and in spinach, but also here the maximum is more to the red in *C.r.* than in spinach (687 vs. 683 nm). This component represents the emission coming from chlorophylls in the core antenna proteins CP47 and CP43 that at 77 K transfer their energy in ~0.5 ns to the photochemical trap and cause the majority of the well-known F685 emission of PSII (43). PSII-3 represents the emission coming mostly from F695, a low lying trap in CP47, which gives isolated PSII its characteristic steady-state emission peak around 695 nm. Upon the S1c → S2c transition the population profiles associated with the three PSII compartments decrease significantly (Fig. 4 *C*). The model quantifies that the total amount of excitations reaching PSII decreases from 71% in S1c to 10% in S2c (Table 1). The respective change upon the S1nc → S2nc transition is less pronounced (Fig. S6 *C*) and decreases from 72% in S1nc (data not shown) to 39% in S2nc (Table 1).

PSI

In *C.r.* nine LHCI antenna proteins are part of the PSI complex (45), which absorbs ~25% of the 475 nm light both in state 1 and in state 2 (see foregoing calculation). Fig. 4, *E* and *F*, represent respectively the dynamics and spectral evolution of the PSI compartments. PSI is characterized by the emission coming from so-called red chlorophylls, excitation traps in the PSI core complex, and the LHCI antenna that are in equilibrium with the excited bulk chlorophylls of the PSI core. PSI-1 represents short-lived emission coming from peripheral and core antenna chlorophylls emitting at ~680 nm, 29% of this PSI-1 is trapped by charge separation in ~26 ps (Fig. 3). A similar phase with a slightly longer lifetime was observed in the target model for 77 K time-resolved emission of thylakoid membranes from spinach (39). The spectrum of PSI-1 peaks at ~679 nm but also has a broad feature around 700 nm, indicating moderately red-shifted chlorophylls from which the excitation energy is rapidly trapped by P700 at 77 K. PSI-2 and PSI-3 are dominated by the characteristic 77 K red Chl emission peaking around 710 and 715 nm, respectively. The lifetimes are ~230 and 820 ps, respectively, and it is possible that these lifetimes are caused by slow uphill energy transfer to the photochemical trap, as was concluded for spinach thylakoid membranes (39). PSI-4 is characterized by a broad band centered at ~725 nm, which presumably arises from extra red-shifted chlorophyll states due to heterogeneity in the energy distribution of the pigments. Only a small fraction of the PSI excitation ends up in this state but due to the long lifetime of 3.4 ns it contributes substantially to the steady-state emission spectrum. The total amount of excitations reaching PSI increases from 28% in S1c (and in S1nc—data not shown) to 70% in S2c and to 44% in S2nc (Table 1).

X-685

In addition to the LHCII, PSI, and PSII components, an unknown state termed X-685 was introduced, after its characteristic emission at 685 nm appearing in the 6 K emission spectra (see the Supporting Material and Fig. S2). X-685 is ST-dependent—its contribution increases significantly from S1c to S2c (and slightly less upon the S1nc → S2nc transition). Note that if it was somehow functionally related to PSII it would show a decrease in amplitude upon the S1 → S2 transition, whereas it does exactly the opposite. It largely decays in 280 ps, but a small fraction has a lifetime of $\approx$6 ns. The X-685 state is in line with the observation of (25) and (26) that not all LHCII lost from PSII is functionally attached to PSI under S2 conditions. The model predicts that 20% of the light is absorbed by X-685 in S2c (respectively 17% in S2nc; Table 1). If X-685 is a special red-shifted LHCII population and if 69% of the light is absorbed by 7-8 LHCII trimers in S1 (see above) then the number of LHCII trimers in the X-685 state is about two per photosynthetic unit. The slight red-shift of X-685 in comparison to bulk LHCII is discussed below. The dynamics and spectral evolution of the X-685 compartment upon the S1c → S2c transition are shown in Fig. 4, *A* and *B*, and upon the S1nc → S2nc transition in Fig. S6, *A* and *B*. The emission from this compartment peaks sharply at 685 nm and it likely has a vibrational tail that is very hard to resolve. Due to its partially long-lived character, the 685-nm band plays an important role in the steady-state emission in S2. To further quantify this, the steady-state emission spectra computed from the target model are depicted in Fig. S7 and discussed in the Supporting Material.

DISCUSSION

X-685 is caused by uncoupled LHCII in S2

In this study, we quantify the extent of ST in intact cells of the green alga *C.r.* by analysis of time-resolved fluorescence at 77 K, and we describe the energy transfer kinetics and yields between the major pigment-protein complexes LHCII, PSI, and PSII. One of the major findings is that

we identified a new, to our knowledge, fluorescence emission band peaking at 685 nm that appeared under state 2 conditions (S2c and S2nc) and that we denoted X-685. Its presence became apparent through a deconvolution of the steady-state fluorescence spectra at 6 K of thylakoids isolated from *C.r.* poised in S2 (Fig. S2 *B*), whereas it did not appear in S1 (Fig. S2 *A*). Similarly, introduction of the X-685 component was essential in the target analysis of the time-resolved fluorescence data at 77 K (Table 1 and Fig. 3). The majority of X-685 decayed with a lifetime of 280 ps and only a small part of X-685 decayed in 5.8 ns. The short-lived component exhibits a strong ST-dependence, appearing only in state 2 and absorbing 18% (S2c; Fig. 3) or 15% (S2nc, data not shown) of all 475 nm excitations. The population of long-lived X-685 reached only 2% in S2c and S2nc, however, due to its long lifetime it contributes considerably to the steady-state fluorescence spectrum (*red* in Fig. S7).

We interpret X-685 as a special form of LHCII that is not able to transfer energy to either PSII or PSI. However, this pool of unbound LHCII emits at 685 nm, whereas the pool of bulk LHCII complexes that do transfer energy to PSII and/or PSI emits fluorescence at around 681 nm (Fig. 4). We suggest that this red-shift of $\approx$4 nm originates from inhomogeneous broadening, which is a consequence of the variation in the spectral forms of chlorophylls among various LHCII monomers. Thus, at low temperature excitation energy migrating between strongly connected LHCIIs will be trapped on one of the red-most forms of chlorophyll. An increase of the number of connected LHCII complexes will result in a larger probability to find red-shifted chlorophylls and thus will result in a red-shifted emission spectrum. The probability of such an event increases with the size of the aggregate, therefore we hardly observe this component in S1, where LHCII-only areas are rare and all LHCII complexes transfer energy quickly to one of the PSs and must all be located near a PS.

In previous studies, spectroscopic properties were compared of trimeric and artificially aggregated forms of LHCII (46–49). In these studies substantial red-shifts to >700 nm were reported of emission maxima at 77 K. However, it is difficult to relate these studies to results observed on LHCII embedded in intact cells, because in artificial aggregates up-and-down faced aggregates will also occur (like in LHCII crystals, see (50)), whereas in vivo all complexes will have the same orientation. On the other hand, single-molecule spectroscopy measurements at room temperature (51) have indicated that trimeric LHCII complexes have a small probability to give rise to red emission, suggesting that also in LHCII-only domains in vivo some red-shifted emission is expected. Therefore, if LHCII-only domains in state 2 would give rise to at least some emission at ~700 nm, and if this emission is equally quenched as X-685, its properties will be very similar to those of the PSI-2 component, that peaks at ~708 nm and decays in ~230 ps (Fig. 3). With target analysis of this data, it is not possible to separate this contribution from PSI and this possible contribution from LHCII-only domains, because their spectra and lifetimes are rather similar. Nevertheless, the fact that PSI-2 also appears in state 1 and does not have a significantly larger amplitude in state 2 compared to the other PSI decay components suggests that a possible contribution of aggregated LHCII in PSI-2 is not more than marginal.

Our results on the lifetime of uncoupled LHCII at 77 K are comparable to those of other authors obtained at room temperature. Iwai et al. (30) measured a lifetime of $\approx$250 ps by fluorescence lifetime imaging microscopy studies on intact *C.r.* and assigned this lifetime to strongly quenched LHCII. Using the same method Unlu et al. (25) reported a lifetime of 400 ps and also explained its origin by strongly quenched uncoupled LHCII. Furthermore, Nagy et al. (26) suggested a pool of phosphorylated unbound LHCII in S2. Therefore, our results confirm the kinetics reported in these earlier studies and in addition provide a spectroscopic fingerprint at cryogenic temperatures.

In the past, 77 K emission spectra have been used as a tool to estimate the extent of the state transition. Emission bands at 715–735 nm have been typically assigned to PSI, whereas emission bands at 695 and 685 nm (F695 and F685) were identified as originating from PSII. Our results on X-685 suggest that at least in *C.r.* the situation is more complex, because uncoupled antenna complexes in S2 will give increased emission around 685 nm. Therefore, the changed emission at 685 nm upon the S1 $\rightarrow$ S2 transition results from two counteracting effects: decrease of PSII emission and increase of X-685 emission.

Properties of state 1 and state 2 obtained with or without chemicals

We induced state 1 either by strong aeration in the dark for 90 min in the presence of the kinase inhibitor 0.1 μM staurosporine (S1c) (32), or by strong aeration for 30 min under >720 nm light without staurosporine (S1nc). Both the 77 K steady-state emission spectra and the target analysis of the 77 K time-resolved data showed no significant differences, from which we conclude that both methods give rise to the same state S1, in which $\approx$95% of LHCII transfers its excitation energy to PSII, $\approx$5% to PSI and in which virtually all excitation energy absorbed by LHCII is directed toward one of the PSs (Table 1). The small extent of energy transfer from LHCII to PSI and the large extent of energy transfer from LHCII to PSII is consistent with an organization as a stacked thylakoid membrane, with LHCII and PSII in the grana membranes and PSI in the stroma lamellae.

State 2 was also induced in two different ways: cells were incubated 45 min under anaerobic conditions in the dark (S2nc), or under the same conditions but with 0.1 M sodium fluoride to inhibit dephosphorylation of LHCII (S2c). In this

case, however, both ways lead to quantitatively different results. Without sodium fluoride, about half of all LHCII transfers its energy to PSII and about a quarter to PSI, whereas another quarter does not transfer its energy to any PS and ends up in X-685 (Table 1). Similar increase of PSI antenna was reported by Nagy et al. who also applied anaerobic conditions to induce S2 (26). This change was paralleled by a decrease of PSII antenna somewhat larger than in this study (50% vs. 32%).The authors concluded therefore that a part of LHCII disconnects from the PSs and forms LHCII-only arrays that rapidly dissipate excitation energy. Unlu et al. induced S2 in a similar way and analyzed the measured time-resolved fluorescence globally reaching a rather qualitative conclusion that a significant amount of LHCII detaches from PSII in S2, but the functional binding of LHCII to PSI is minimal (25). However, Drop et al. (31,44), performing an electron microscopy analysis of supercomplexes derived from *C.r.* revealed characteristic PSII-LHCII supercomplexes (44) and in the cells poised in S2 also substantial amounts of a PSI-LHCI-LHCII supercomplex that binds two trimeric LHCII units per PSI (31), consistent with our results on S2nc in which ~20% of all LHCII trimers is functionally attached to PSI. Overall, the results of our 77 K study are in rather good agreement with the recent works performed at room temperature by Unlu et al. and Nagy et al.; however, these different temperature regimes and different applied measuring techniques might lead to some minor discrepancies in the drawn conclusions. Similar to these two studies, we provide evidence of a pool of uncoupled LHCII, which was also suggested before by Minagawa et al. (27). Strikingly, the existence of this pool was excluded in another room temperature study where the pool of mobile LHCII complexes was estimated to 80% (16). In our study, by applying target analysis and combining it with the knowledge from GA, 6 K steady-state spectra and previous structural studies we can additionally characterize kinetics and spectral properties of these free LHCII complexes and draw a quantitative picture of excitation energy distribution between PSI, PSII, and free LHCII and how it changes upon ST.

With 0.1 M sodium fluoride (32), a very different state was obtained (designated S2c). Although the amount of X-685 does not differ very much (adding sodium fluoride increased the relative amount of excitations absorbed by X-685 from ~17% to ~20%, see Table 1), the number of LHCII functionally associated with PSII or PSI changed very drastically, with almost all LHCII trimers transferring now the excitation energy to PSI. Thus, the extent of ST, or the functional connection of LHCII to either PSII in S1 or to PSI in S2 is much larger now and is even almost complete as almost no LHCII is functionally connected to PSI in S1 and almost no LHCII is connected to PSII in S2. However, the addition of 0.1 M sodium fluoride is a drastic treatment, and it is very well possible that this treatment causes more effects on the physiology of *C.r.* than just inhibiting the phosphatase involved in the dephosphorylation of LHCII. Hence, the question is justified in which respect the extended state transition brought about by this treatment is meaningful for the understanding of this regulatory process. On the other hand, based on fluorescence measurements there are no signs that hint at damaged or deteriorated pigment-protein complexes, like the occurrence of free pigments emitting with high quantum yield at short wavelengths. The simplest interpretation of the results is that the addition of 0.1 M sodium phosphate in anaerobic conditions leads to a membrane organization by which most LHCII transfers its excitation energy to PSI, a smaller part of absorbed energy is rapidly lost in an LHCII-only domain and only a very small part of the energy is transferred to PSII. Therefore, although without sodium fluoride the thylakoid membranes are thought to occur in a partially stacked/unstacked organization (26), the addition of 0.1 M sodium fluoride in anaerobic conditions could lead to a completely unstacked thylakoid membrane organization, because only in this case the very small extent of energy transfer from LHCII to PSII can be explained. The target analysis of 77 K time-resolved emission of unstacked thylakoid membranes from spinach (39) gave very similar results with regard to the energy transfer from LHCII to PSII, in line with our suggestion that in S2c the membranes are completely unstacked. Moreover, we ruled out any specific influence of sodium fluoride on ST by observing that no difference was present in the 77 K steady-state fluorescence spectra of the *stt7* mutant incubated under conditions, which in WT promoted S1nc, S2nc, or S2c (data not shown).

CONCLUSIONS

The combined results of our work and of others (25,26) suggest that, in most cases, the S2 state consists of two components. The first component is caused by traditionally reported LHCII, which transfers energy to PSII in S1 and to PSI in S2. The second component involves a rearrangement of a part of LHCII that transfers energy to PSII in S1 and appears in LHCII-only domains in S2 that do not transfer energy to any PS and rapidly decay energy by nonphotochemical quenching. Thus, in this case the LHCII has a photoprotective function in S2. The extent of energy transfer efficiency to PSI obviously varies substantially: in the cells prepared by (25), this component is virtually absent, in our S2nc cells this component is small but significant, and in our S2c cells this component is very large. The reason for this variation and the docking sites of the LHCII to PSI requires clearly further studies in the future.

SUPPORTING MATERIAL

Supporting Materials and Methods, seven figures, and one table are available at http://www.biophysj.org/biophysj/supplemental/S0006-3495(14)04683-9.

ACKNOWLEDGMENTS

This work was supported by Marie Curie Initial Training Network HARVEST sponsored by the 7th Framework Programme of the European Union (L.M.W. and J.P.D.; project reference: 238017) and carried out in part within the research programme of BioSolar Cells, cofinanced by the Dutch Ministry of Economic Affairs, Agriculture and Innovation (J.J.S., J.P.D., R.vG., and I.H.M.vS.). R.vG. and I.H.M.vS. acknowledge financial support of the European Research Council (Advanced Grant proposal 267333 (PHOTPROT) to R.vG.). R.vG. gratefully acknowledges his Academy Professorship (Akademie Hoogleraar) from the Royal Netherlands Academy for Arts and Sciences (KNAW).

SUPPORTING CITATIONS

References (52,53) appear in the Supporting Material.

REFERENCES

1. Dekker, J. P., and E. J. Boekema. 2005. Supramolecular organization of thylakoid membrane proteins in green plants. *Biochim. Biophys. Acta.* 1706:12–39.
2. van Grondelle, R., and V. I. Novoderezhkin. 2006. Energy transfer in photosynthesis: experimental insights and quantitative models. *Phys. Chem. Chem. Phys.* 8:793–807.
3. Novoderezhkin, V. I., and R. van Grondelle. 2010. Physical origins and models of energy transfer in photosynthetic light-harvesting. *Phys. Chem. Chem. Phys.* 12:7352–7365.
4. van Amerongen, H., and R. Croce. 2013. Light harvesting in photosystem II. *Photosynth. Res.* 116:251–263.
5. Croce, R., and H. van Amerongen. 2013. Light-harvesting in photosystem I. *Photosynth. Res.* 116:153–166.
6. Murata, N. 1969. Control of excitation transfer in photosynthesis. I. Light-induced change of chlorophyll a fluorescence in *Porphyridium cruentum*. *Biochim. Biophys. Acta.* 172:242–251.
7. Bonaventura, C., and J. Myers. 1969. Fluorescence and oxygen evolution from *Chlorella pyrenoidosa*. *Biochim. Biophys. Acta.* 189:366–383.
8. Allen, J. F. 1992. Protein phosphorylation in regulation of photosynthesis. *Biochim. Biophys. Acta.* 1098:275–335.
9. Wollman, F.-A., and C. Lemaire. 1988. Studies on kinase-controlled state transitions in photosystem II and *b6f* mutants from *Chlamydomonas reinhardtii* which lack quinone-binding proteins. *Biochim. Biophys. Acta.* 933:85–94.
10. Allen, J. F., J. Bennett, …, C. J. Arntzen. 1981. Chloroplast protein phosphorylation couples plastoquinone redox state to distribution of excitation energy between photosystems. *Nature.* 291:25–29.
11. Depège, N., S. Bellafiore, and J.-D. Rochaix. 2003. Role of chloroplast protein kinase *Stt7* in LHCII phosphorylation and state transition in *Chlamydomonas*. *Science.* 299:1572–1575.
12. Silverstein, T., L. Cheng, and J. F. Allen. 1993. Chloroplast thylakoid protein phosphatase reactions are redox-independent and kinetically heterogeneous. *FEBS Lett.* 334:101–105.
13. Samol, I., A. Shapiguzov, …, M. Goldschmidt-Clermont. 2012. Identification of a photosystem II phosphatase involved in light acclimation in *Arabidopsis*. *Plant Cell.* 24:2596–2609.
14. Rochaix, J.-D. 2001. Assembly, function, and dynamics of the photosynthetic machinery in *Chlamydomonas reinhardtii*. *Plant Physiol.* 127:1394–1398.
15. Finazzi, G. 2005. The central role of the green alga *Chlamydomonas reinhardtii* in revealing the mechanism of state transitions. *J. Exp. Bot.* 56:383–388.
16. Delosme, R., J. Olive, and F.-A. Wollman. 1996. Changes in light energy distribution upon state transitions: an in vivo photoacoustic study of the wild type and photosynthesis mutants from *Chlamydomonas reinhardtii*. *Biochim. Biophys. Acta.* 1273:150–158.
17. Goodenough, U. W., and R. P. Levine. 1969. Chloroplast ultrastructure in mutant strains of *Chlamydomonas reinhardtii* lacking components of the photosynthetic apparatus. *Plant Physiol.* 44:990–1000.
18. Bertos, N. R., and S. P. Gibbs. 1998. Evidence for a lack of photosystem segregation in *Chlamydomonas reinhardtii* (Chlorophyceae). *J. Phycol.* 34:1009–1016.
19. Kargul, J., M. V. Turkina, …, J. Barber. 2005. Light-harvesting complex II protein CP29 binds to photosystem I of *Chlamydomonas reinhardtii* under State 2 conditions. *FEBS J.* 272:4797–4806.
20. Tokutsu, R., M. Iwai, and J. Minagawa. 2009. CP29, a monomeric light-harvesting complex II protein, is essential for state transitions in *Chlamydomonas reinhardtii*. *J. Biol. Chem.* 284:7777–7782.
21. Kouril, R., A. Zygadlo, …, E. J. Boekema. 2005. Structural characterization of a complex of photosystem I and light-harvesting complex II of *Arabidopsis thaliana*. *Biochemistry.* 44:10935–10940.
22. Bulté, L., P. Gans, …, F.-A. Wollman. 1990. ATP control on state transitions in vivo in *Chlamydomonas reinhardtii*. *Biochim. Biophys. Acta.* 1020:72–80.
23. Finazzi, G., A. Furia, …, G. Forti. 1999. State transitions, cyclic and linear electron transport and photophosphorylation in *Chlamydomonas reinhardtii*. *Biochim. Biophys. Acta.* 1413:117–129.
24. Takahashi, H., S. Clowez, …, F. Rappaport. 2013. Cyclic electron flow is redox-controlled but independent of state transition. *Nat. Commun.* 4:1954.
25. Ünlü, C., B. Drop, …, H. van Amerongen. 2014. State transitions in *Chlamydomonas reinhardtii* strongly modulate the functional size of photosystem II but not of photosystem I. *Proc. Natl. Acad. Sci. USA.* 111:3460–3465.
26. Nagy, G., R. Ünnep, …, J. Minagawa. 2014. Chloroplast remodeling during state transitions in *Chlamydomonas reinhardtii* as revealed by noninvasive techniques in vivo. *Proc. Natl. Acad. Sci. USA.* 111:5042–5047.
27. Minagawa, J. 2011. State transitions—the molecular remodeling of photosynthetic supercomplexes that controls energy flow in the chloroplast. *Biochim. Biophys. Acta.* 1807:897–905.
28. Ruban, A. V., R. Berera, …, R. van Grondelle. 2007. Identification of a mechanism of photoprotective energy dissipation in higher plants. *Nature.* 450:575–578.
29. van Stokkum, I. H. M., B. van Oort, F. van Mourik, B. Gobets, and H. van Amerongen. 2008. (Sub)-picosecond spectral evolution of fluorescence studied with a synchroscan streak-camera system. *In* Biophysical Techniques in Photosynthesis II. T. J. Aartsma and J. Matysik, editors.. Springer, pp. 223–240.
30. Iwai, M., M. Yokono, …, J. Minagawa. 2010. Live-cell imaging of photosystem II antenna dissociation during state transitions. *Proc. Natl. Acad. Sci. USA.* 107:2337–2342.
31. Drop, B., S. Yadav K N, …, R. Croce. 2014. Consequences of state transitions on the structural and functional organization of photosystem I in the green alga *Chlamydomonas reinhardtii*. *Plant J.* 78:181–191.
32. Takahashi, H., M. Iwai, …, J. Minagawa. 2006. Identification of the mobile light-harvesting complex II polypeptides for state transitions in *Chlamydomonas reinhardtii*. *Proc. Natl. Acad. Sci. USA.* 103:477–482.
33. Subramanyam, R., C. Jolley, …, A. N. Webber. 2006. Characterization of a novel Photosystem I-LHCI supercomplex isolated from *Chlamydomonas reinhardtii* under anaerobic (State II) conditions. *FEBS Lett.* 580:233–238.
34. Cardol, P., G. Gloire, …, F. Franck. 2003. Photosynthesis and state transitions in mitochondrial mutants of *Chlamydomonas reinhardtii* affected in respiration. *Plant Physiol.* 133:2010–2020.
35. Alric, J. 2010. Cyclic electron flow around photosystem I in unicellular green algae. *Photosynth. Res.* 106:47–56.

36. Rebéillé, F., and P. Gans. 1988. Interaction between chloroplasts and mitochondria in microalgae: role of glycolysis. *Plant Physiol.* 88:973–975.

37. Mus, F., A. Dubini, …, A. R. Grossman. 2007. Anaerobic acclimation in *Chlamydomonas reinhardtii*: anoxic gene expression, hydrogenase induction, and metabolic pathways. *J. Biol. Chem.* 282:25475–25486.

38. van Stokkum, I. H. M., D. S. Larsen, and R. van Grondelle. 2004. Global and target analysis of time-resolved spectra. *Biochim. Biophys. Acta.* 1657:82–104.

39. Snellenburg, J. J., J. P. Dekker, …, I. H. M. van Stokkum. 2013. Functional compartmental modeling of the photosystems in the thylakoid membrane at 77 K. *J. Phys. Chem. B.* 117:11363–11371.

40. Snellenburg, J. J., S. P. Laptenok, …, I. H. M. van Stokkum. 2012. Glotaran: a Java -based graphical user interface for the R-package TIMP. *J. Stat. Softw.* 49:1–23.

41. van der Weij-de Wit, C. D., J. A. Ihalainen, …, J. P. Dekker. 2007. Excitation energy transfer in native and unstacked thylakoid membranes studied by low temperature and ultrafast fluorescence spectroscopy. *Photosynth. Res.* 93:173–182.

42. van der Weij-de Wit, C. D., J. P. Dekker, …, I. H. van Stokkum. 2011. Charge separation is virtually irreversible in photosystem II core complexes with oxidized primary quinone acceptor. *J. Phys. Chem. A.* 115:3947–3956.

43. Andrizhiyevskaya, E. G., A. Chojnicka, …, J. P. Dekker. 2005. Origin of the F685 and F695 fluorescence in photosystem II. *Photosynth. Res.* 84:173–180.

44. Drop, B., M. Webber-Birungi, …, R. Croce. 2014. Light-harvesting complex II (LHCII) and its supramolecular organization in *Chlamydomonas reinhardtii*. *Biochim. Biophys. Acta.* 1837:63–72.

45. Drop, B., M. Webber-Birungi, …, R. Croce. 2011. Photosystem I of *Chlamydomonas reinhardtii* contains nine light-harvesting complexes (Lhca) located on one side of the core. *J. Biol. Chem.* 286:44878–44887.

46. Ruban, A. V., J. P. Dekker, …, R. van Grondelle. 1995. Temperature-dependence of chlorophyll fluorescence from the light-harvesting complex Ii of higher-plants. *Photochem. Photobiol.* 61:216–221.

47. Horton, P., and A. V. Ruban. 1992. Regulation of photosystem II. *Photosynth. Res.* 34:375–385.

48. Mullineaux, C. W., A. a. Pascal, …, A. R. Holzwarth. 1993. Excitation-energy quenching in aggregates of the LHC II chlorophyll-protein complex: a time-resolved fluorescence study. *Biochim. Biophys. Acta.* 1141:23–28.

49. Johnson, M. P., and A. V. Ruban. 2009. Photoprotective energy dissipation in higher plants involves alteration of the excited state energy of the emitting chlorophyll(s) in the light harvesting antenna II (LHCII). *J. Biol. Chem.* 284:23592–23601.

50. Kühlbrandt, W., T. Thaler, and E. Wehrli. 1983. The structure of membrane crystals of the light-harvesting chlorophyll a/b protein complex. *J. Cell Biol.* 96:1414–1424.

51. Krüger, T. P. J., V. I. Novoderezhkin, …, R. van Grondelle. 2010. Fluorescence spectral dynamics of single LHCII trimers. *Biophys. J.* 98:3093–3101.

52. Germano, M., A. E. Yakushevska, …, E. J. Boekema. 2002. Supramolecular organization of photosystem I and light-harvesting complex I in *Chlamydomonas reinhardtii*. *FEBS Lett.* 525:121–125.

53. Hemelrijk, P. W., S. L. S. Kwa, …, J. P. Dekker. 1992. Spectroscopic properties of LHC-II, the main light-harvesting chlorophyll a/b protein complex from chloroplast membranes. *Biochim. Biophys. Acta.* 1098:159–166.